Time-Delay Study of Earth Orientation Parameters at Inter-Annual Time Scales

P. Manneville

Laboratoire d'Hydrodynamique (LadHyX), École polytechnique, F-91128 Palaiseau cedex, France

E-mail: paul.manneville@ladhyx.polytechnique.fr

(Received 31 January 2001)

We proceed to a reanalysis of time series of the Earth Orientation Parameters available from IERS [4] using Takens' time-delay embedding technique [5]. Focusing on intermediate time scales rather than short ones as done in [3], we extract oscillations corresponding to Chandler wobble by singular-value decomposition [7] of the time-series of the Celestial Ephemeris Pole position (PMX,PMY) on the period 1890–2000. A π phase-shift of the oscillation around 1930 is pointed out explicitly. A similar study of the length-of-day time series shows strong correlation with indices measuring the strength of the ENSO phenomenon on the period 1962–1999 [23]. Differences between the dynamical systems approach and conventional signal analyses are emphasized.

Key words: time series, Earth Orientation Parameters, Takens' time-delay embedding technique, ENSO phenomenon

PACS numbers: 05.45.T; 95.75.W

1 Introduction

Phase-space reconstruction techniques developed in the theory of low-dimensional deterministic dynamical systems are now currently used as signal processing tools [1, 2]. In the present paper, following V. Frède's seminal work [3], we consider data series of the fluctuations of the Earth's orientation parameters (EOP in the following) and take them as an interesting case study in this framework.

The EOP can be measured with precision since the end of the XIX$^{\text{th}}$ Century and even more so with the development of spatial techniques. A better understanding of EOP variations has much interest from both theoretical (origin of fluctuations) and applied (improvement of positioning) viewpoints. Original data are available from the *International Earth Rotation Service* (IERS) at Paris observatory [4]. They describe the fine details of the rotation of the Earth about its axis. As a matter of fact, like any solid object rotating around an axis that is not rigorously along one of its inertia axes, the Earth experiences a *nutation* , i.e. a motion of the direction of the relevant inertia axis in an absolute frame or, equivalently, an apparent motion of the rotation axis in a body-fixed reference frame. A large part of this motion is accessible to astronomical computation but a part remains that turns out to be not fully regular. In the same way, once computable corrections linked to tide effects on the equatorial bulge have been subtracted, the length of the day (LOD in the following) also fluctuates around its average value.

In the following section we present the data to be studied in little more detail. The next section is devoted to a sketchy description of the tools we shall make use of, Takens' *time delay technique* [5] rooting new approaches to data processing, and filtering by singular value decomposition [6, 7]. In her PhD work, V. Fréde focused her attention on the high frequency dynamics of the EOP (from days to months). In particular, from phase-space recon-

structions she attempted to characterize the predictability of the time series, and to correlate it with the El Niño climatic oscillation at a qualitative level. By contrast, we shall consider fluctuations on inter-annual time scales, for which we believe that the techniques used are even more effective. We shall study first, §4, the motion of the pole axis and more specifically the oscillation known as the *Chandler wobble* , and next, §5, the LOD variations showing quantitative correlation with the climatic oscillation mentioned above. While not trying to substitute ourselves to specialists of the different scientific disciplines concerned, astronomy, geodesy, geophysics, or climatology, in the final section we shall discuss —perhaps too naively— what can be learned from the abstract approaches deriving from dynamical systems theory.

2 The Earth's orientation parameters (EOP)

As a matter of principle, the kinematics of the Earth should be described in an inertial frame linked to the stars, defined by convention as the *International Celestial Reference System* (ICRS). All measurements performed on Earth are however rather expressed in a geocentric frame linked to its solid crust, the *International Terrestrial Reference System* (ITRS). One of its axes defines the *IERS Reference Pole* (IRP) while another one helps us specifying the *IERS Reference Meridian* (IRM). In order to be able to account for the kinematics of the Earth's rotation [8], one must know how to pass from one reference frame to the other. Theoretically, the orientation of a frame rigidly linked to an arbitrarily shaped solid depends on three parameters, e.g. Euler's angles. From the astronomical point of view, the Earth rotates around a conventional reference axis that defines a pole called the *Celestial Ephemeris Pole* (CEP). The motion of the CEP is determined from its coordinates PMX and PMY in a frame linked to the IRP. The third parameter is a longitude that permanently grows with time and will be related to the length of the day (LOD).

Considering an average Earth supposed to be a solid of invariable shape, one can account for the motion of the CEP of astronomical origin by means of precession-nutation models. This motion is due to gravitational effects of other celestial bodies on the equatorial bulge induced by centrifugal forces. Models predict a motion that can be subtracted from the observations but measurements are sufficiently precise that irregular residual deviations show up. (In fact, models are imperfect and two tiny quasi-periodic empirical corrections $\delta\psi$ and $\delta\epsilon$ must be introduced, corresponding to systematic longitude and obliquity shifts of the CEP's position. They will be neglected in the following.)

The interpretation of the fact that the CEP experiences motions not predicted by the astronomical precession-nutation theory stems from the observation that, at time scales of interest, the Earth is a deformable body made of a solid part with complex interior and two fluid parts, the oceans and the atmosphere. Inertia parameters of the solid part may slightly vary as its shape changes, while the fluid envelopes permanently exchange angular momentum with it. Earthquakes, interactions between the Earth's core and mantle, underground water and glacier motions have similar effects. All this generates fluctuations of the CEP position (PMX,PMY) and also of the instantaneous rotation rate to be examined later.

Besides seasonal components, annual and subannual, the CEP orientation fluctuations contains an important contribution called *Chandler wobble* (CW in the following, for a recent overview see [9]). This contribution corresponds to a free nutation motion, the period of which should be 305.5 days if the Earth were a rigid revolution ellipsoid as assumed by Euler who first predicted this motion. In fact the Earth's elasticity lengthens the period to about 433 days and its internal viscosity damps the motion with a characteristic time in the range 30–70 years that is more difficult to estimate. At any rate, the oscillation should have disappeared if it were not permanently excited. Different mechanisms have been advocated for this excitation, see [10] for a recent contribution concluding that, at least in the last 20 years, the pressure fluctuations at the bottom of the oceans are responsible for a

large part of it.

In addition to these orientation fluctuations, the Earth also experiences variations of its instantaneous rotation rate. The universal time UT1 is the time derived from the rotation of the Earth that, by definition, completes one turn in 24 hours, i.e. it give the instantaneous direction of the reference meridian (IMR) and is different from the uniformly flowing sidereal or 'absolute' time as given by, e.g., an atomic clock. From the difference between UT1 and the sidereal time one derives the length of the day (LOD). In addition to the secular slowing down due to the loss of angular momentum by viscous friction, LOD variations also contain a computable multi-periodic contribution linked to tide effects. Once they have been subtracted, what remains is the result of fluctuations of the torque exerted by the other components of the planet (atmosphere, ocean, core) on the solid crust to which the IRM is linked. These fluctuations are present on a wide range of time scales. The origins of the shortest are meteorological or seismic. At the scale of months, regular seasonal climatic variations should certainly be invoked. Here we shall be interested in inter-annual variability most likely also linked to climatic processes such as the celebrated 'El Niño–Southern Oscillation' (ENSO) phenomenon [11].

3 Time-delay signal processing

Takens' time delay technique. Within the framework of dynamical systems theory most signal processing methods derive from Takens' *method of time delays* [5]. This method assumes that the physical system of interest, mathematically described by some (unknown) continuous time differential dynamical system $\frac{d}{dt}\mathbf{X} = \mathbf{F}(\mathbf{X})$ in its (unknown) phase space $\mathbb{X}$ of (unknown) dimension d, produces a discrete time series $W_k = W(t_k)$, $k = 0, 1, 2, \ldots$, by sampling of some observable $W(t) = \mathcal{W}(\mathbf{X}(t))$ at regularly spaced times $t_k = k\tau$. The system is then represented in a space $\mathbb{Y} = \mathbb{R}^{d_e}$ by discrete trajectory points $\mathbf{Y}_k$, $k = 0, 1, 2, \ldots$ with sub-series of d_e consecutive measurements as coordinates:

$$\mathbf{Y}_k \equiv [W_k, W_{k+1}, \ldots W_{k+d_e-1}]' \qquad (1)$$

where the prime indicates transposition to fit with the convention of denoting vectors as column arrays. From a theoretical point of view, mathematical *embedding* theorems guarantee the faithfulness of this representation provided that the dimension d_e is taken large enough (see [12] for a review). But these theorems hold in the ideal case of noiseless data and do not solve the empirical problems of finding the most appropriate sampling time τ and choosing the embedding dimension most efficiently. Prescriptions for τ have been given, e.g. take the value giving the first relative minimum of the *mutual information* between delayed coordinates $W(t)$ and $W(t+\tau)$ [13]. Strategies have also been developed to go beyond the simple trial-and-error method that consist of increasing d_e up to the point where stable results are obtained, the *false near-neighbor method* is one such strategy [14]. Dynamical information can then be extracted from the reconstruction, e.g. Lyapunov exponents and fractal dimensions; see [1, 2] for details and concrete implementations.

Using singular value decomposition (SVD). In practice, the canonical basis of space $\mathbb{Y}$ is not optimal in the sense that a circular permutation of the axes leaves the reconstruction invariant. It may thus be interesting to turn to a different basis better correlated to the data *in the least-square sense.* This is done by considering the correlation between a given reconstructed vector state $\mathbf{Y}_k$ and an arbitrary test vector $\mathbf{Z}$, measured by the square of the scalar product $\mathbf{Y}_k \cdot \mathbf{Z}$ and minimizing the quantity

$$\sum_{k=1}^{n_v} (\mathbf{Y}_k \cdot \mathbf{Z})^2 \qquad (2)$$

where $n_v = n_t - d_e$, n_t being the total number of measurements and n_v the number of reconstructed vectors. This directly leads [6] to an eigen-value problem for the covariance matrix R, with coefficients

$$R_{mm'} = R_{m'm} = \frac{1}{n_v} \sum_{k=1}^{n_v} W_{k+m-1} W_{k+m'-1},$$

for example: $R_{11} = (1/n_v)\sum_{k=1}^{n_v} W_k^2$, $R_{12} = R_{21} = (1/n_v)\sum_{k=1}^{n_v} W_k W_{k+1}$, etc. This symmetric matrix, definite and positive by construction, can thus be diagonalized. Its spectrum can be ordered by decreasing values, the largest ones corresponding to that part of the motion containing most of the variance of the signal. It can be shown [6] that the searched spectrum is nothing but the square of the singular spectrum obtained from the *singular value decomposition* (SVD) of the 'trajectory matrix' with coefficients $T_{mm'} = W_{m+m'-1}$, which is routinely achieved by efficient algorithms. Furthermore, the eigen-vectors of the covariance matrix form an orthogonal basis of the d_e-dimensional reconstruction space $\mathbb{Y}$ on which trajectories can be projected. A feature of the decomposition, to be illustrated later, is the presence of quasi-degenerated pairs of eigenvalues with associated wave-vectors out of phase by $\pi/2$ when the signal hides a possibly strong, but modulated or even intermittent, periodic component at some frequency [7], which opens the possibility of selective reconstruction, i.e. adaptive filtering. Though the system can be further studied in the so-selected eigen-subspaces [6], it is often interesting to recompose the filtered signal in the canonical basis, that is to say, to write it back as a time series (i.e. to find the trajectory matrix corresponding to the filtered principal components), which can be done approximately in the least-square sense, as shown in [7].

Hilbert transform and demodulation. As will happen to be the case here, it is often useful to extract the amplitude and the phase of signals displaying strong periodicities. This can be done elegantly by constructing the *analytic* signal $W_c(t) = W(t) + iW_\perp(t)$ associated to the given real signal $W(t)$. The imaginary part $W_\perp(t)$ is constructed to be out of phase by $\pi/2$ with W by means of the Hilbert transform: $\hat{W}_\perp(\omega) = -(1/\pi)\mathcal{P}\int_{-\infty}^{\infty} d\omega' \hat{W}(\omega')/(\omega - \omega')$, where $\hat{F}(\omega)$ is the Fourier transform of $F(t)$ and $\mathcal{P}$ denotes the Cauchy principal part of the integral [15]. The instantaneous amplitude and phase of the signal are then given by the modulus and the argument of $W_c(t) = |W_c(t)|\exp[i\phi(t)]$, the instantaneous frequency being obtained by differentiating the phase with respect to time. Concretely, the Fourier transform of W_c is obtained from that of W by canceling all its negative frequency components.

4 CEP motion and the Chandler wobble

The PMX and PMY time series, available from the IERS as file C01 [16], contains 2181 data pieces sampling the period 01/01/1890–01/01/1999 at a rate of 20 values per year. Conventionally, the coordinates (PMX,PMY) of the CEP are determined in a frame centered at the IRP, its x axis along the reference meridian, its y axis along meridian W90. In order to recover a direct frame, in the following we study the time series of PMX and $-$PMY, as displayed without any treatment in the two upper panels of figure 1. The trend visible on the figure is likely due to slow geophysical processes. Instead of removing it by subtracting a sliding average, we prefer fitting a polynomial to the raw data, as if the drift was due to some slow but deterministic dynamics that could be represented by the first terms of its Taylor expansion [17]. After subtraction of the trend one gets the data displayed in the two bottom panels of figure 1 that will serve in the following.

Results of a Fourier analysis of the detrended complex time series $Z = X + iY$ are displayed in figure 2. The annual period is clearly identified in the two top panels as corresponding to the sharp intense peak at $n = +109$ and the smaller one at $n = -109$. The Chandler wobble is consistent with the wide peak around $n \sim 92$.

In practice, since the periods of annual and subannual regular fluctuations are known exactly, it turns out to be preferable to eliminate the corresponding signal components by least square fitting the coefficients of few terms of an appropriate Fourier series [17]. The control Fourier spectrum shown in the bottom panel of figure 2 suggests that the result, displayed as a time series in figure 3, is satisfactory in that there seems to remain no trace of the beat between the annual and Chandler frequencies visible in figure 1.

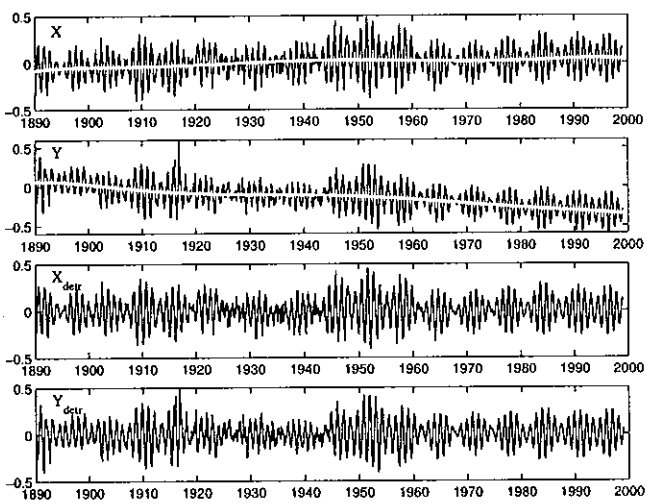

FIG. 1. Time series of the CEP coordinates $X \equiv$ PMX and $Y \equiv -$PMY. Top: Raw data with indication of the trend. Bottom: detrended data.

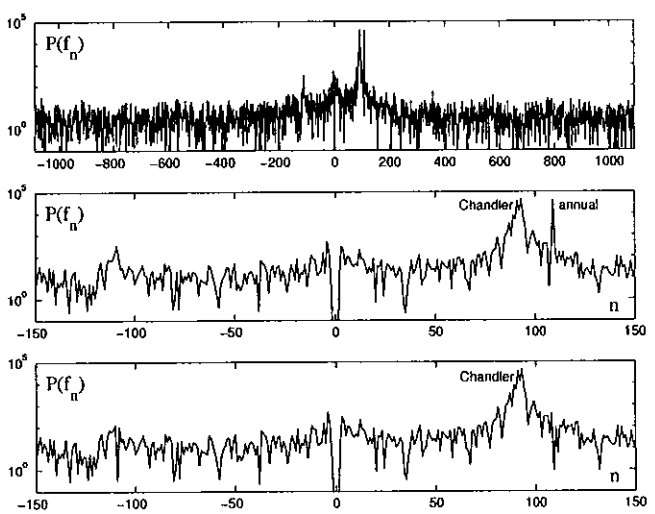

FIG. 2. Fourier spectrum $P(f_n) = |\hat{Z}_n|^2$ of detrended time series of $Z = X + iY$ ($f_n = n/T$ in years^{-1}, $T = 109$). Top: complete spectrum. Middle: zoom on the central part pointing out the annual and Chandler contribution to the spectrum. Bottom: control spectrum after removal of annual Fourier modes.

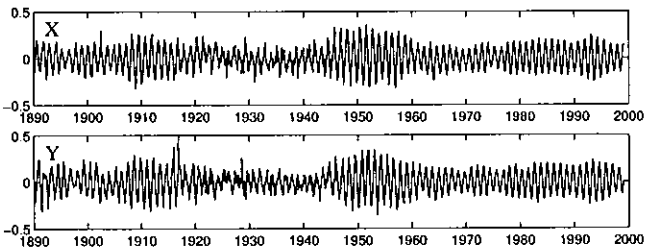

FIG. 3. Time series of detrended X and Y after subtraction of the periodic annual fluctuation.

Let us now study the cleaned time series by the methods briefly described in the previous section. The period of the Chandler wobble is close to 433 days. In order to take a window width (embedding dimension) in resonance with this duration we have taken $d_e = 95$, that is to say very nearly 4 periods ($4 \times 20 \times 433/365 \simeq 94.9$). As seen in figure 4, two singular values representing 86–87% of the variance of the signal emerge from a somewhat undifferentiated background. Furthermore the singular spectra corresponding to coordinates X and Y are essentially identical. The eigen-vectors obtained from the analysis of the X series and corresponding to these two eigen-values are displayed in figure 5. As expected in case of a signal close to periodic and a window length commensurate with the approximate period [7], these two vectors display 4 periods of nearly sinusoidal oscillations out of phase by $\pi/2$ with each other (the latter fact can be checked by comparing one of them with the Hilbert transform of the other). Performing the same work on the Y series one obtain two new eigen-vectors that turn out to fulfill the relations ${V_1}^{(X)} = {V_2}^{(Y)}$ and ${V_2}^{(X)} = -{V_1}^{(Y)}$ (quantitatively, denoting the Euclidean norm as $\| \ \|_2$, one has $\|{V_1}^{(X)} - {V_2}^{(Y)}\|_2 / \|{V_1}^{(X)}\|_2$ and $\|{V_2}^{(X)} + {V_1}^{(Y)}\|_2 / \|{V_2}^{(X)}\|_2$ both less than 2%). All this confirms that X and Y are two components of a single periodic (but modulated) behavior best studied in the complex plane $Z = X + iY$.

Filtering the series by keeping the principal components corresponding to the two first vectors $(X_{1\text{-}2}, Y_{1\text{-}2})$ or on the contrary to all other vectors $(X_{3\text{-}95}, Y_{3\text{-}95})$ and recomposing the time series as in

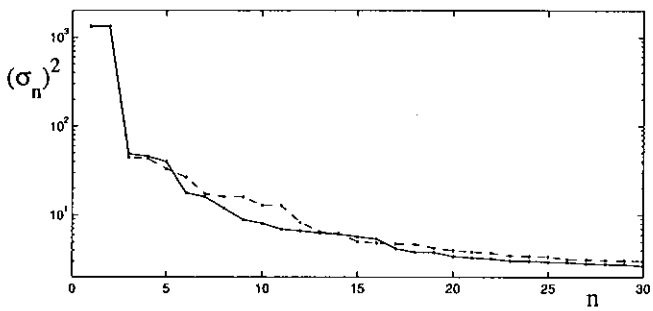

FIG. 4. Head of the spectrum σ_n^2 of the covariance matrix with embedding dimension $d_e = 95$ (solid and dashed lines for X and Y, respectively).

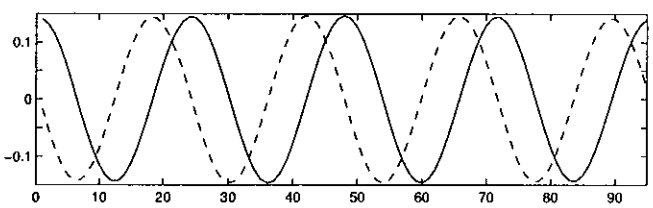

FIG. 5. The two first eigen-vectors issued from the analysis of the X time series.

[7] yields the signals illustrated in figure 6. Fourier analysis further shows that except for a small contribution at modes close to -109 originating from a slight modulation of fluctuations at annual and subannual periods (that could not be eliminated by a procedure adapted to a strictly periodic signal), the spectrum of the residue, principal components 3 to 95, is essentially featureless. This strongly suggests that all the variability associated with the Chandler wobble has been properly extracted and is to be found in components (1–2). Figure 7 displays the corresponding reconstructed trajectory in the complex plane $Z = X_{1\text{-}2} + iY_{1\text{-}2}$, clearly understood as describing a nearly sinusoidal oscillation of variable amplitude and phase, ready for quantitative characterization.

The amplitude of the wobble can first be estimated as a function of time from the modulus of Z. This is done in figure 8 (top) where it can be seen that small, intermittent and fast fluctuations are superimposed on a large, smooth and slow variation. Further examination of the fast fluctuations shows that they are essentially made of spells of harmon-

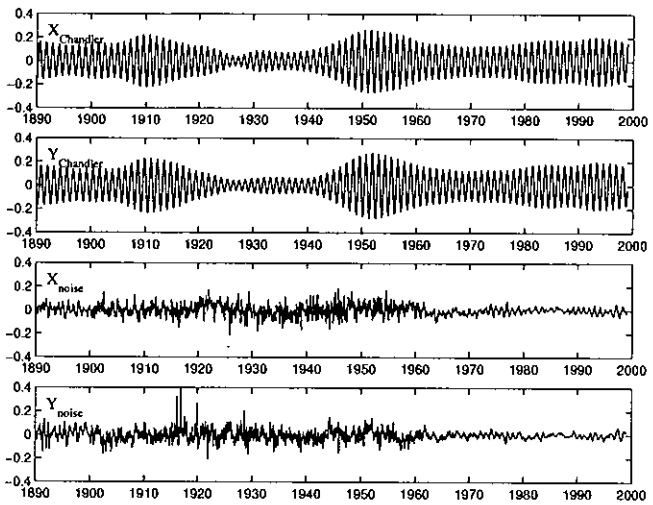

FIG. 6. Recomposed times series. Top: nontrivial Chandler component ($X_{1\text{-}2}$ and $Y_{1\text{-}2}$). Bottom: residue ($X_{3\text{-}95}$, $Y_{3\text{-}95}$).

ics of the basic frequency. In the bottom panel of the same figure the amplitudes of the oscillations of $X_{1\text{-}2}$ and $Y_{1\text{-}2}$, taken separately, are plotted as obtained from the modulus of the analytic signals X_c and Y_c derived by means of the Hilbert transform. While they seem to envelope the variation of $|Z|$, these amplitudes show no trace of the previous fast oscillations [18]. As can be understood from a simple calculation, all this arises because the two signals $X_{1\text{-}2}$ and $Y_{1\text{-}2}$ are nearly but not rigorously out of phase by $\pi/2$.

One may note that the amplitude of the Chandler wobble is particularly small on the interval [1925–1940], with two large humps before and after this period. A small amplitude oscillation with period of the order of 10 years seems to be superimposed on the large amplitude modulation. This oscillation can be made objective by a SVD of the $|Z|$ time series, the results of which will not be presented here since they do not bring more than what can be guessed from visual inspection.

Let us now examine the variations of $\phi = \arg(Z)$ which are directly related to those of the oscillation period. As can be guessed from figure 7, ϕ indeed increases regularly, which is further illustrated in figure 9 (top) where a linear growth $\phi_0 = \omega_0 t$, with $\omega_0 = 2\pi/T_0$, $T_0 = 433$ days, has been subtracted.

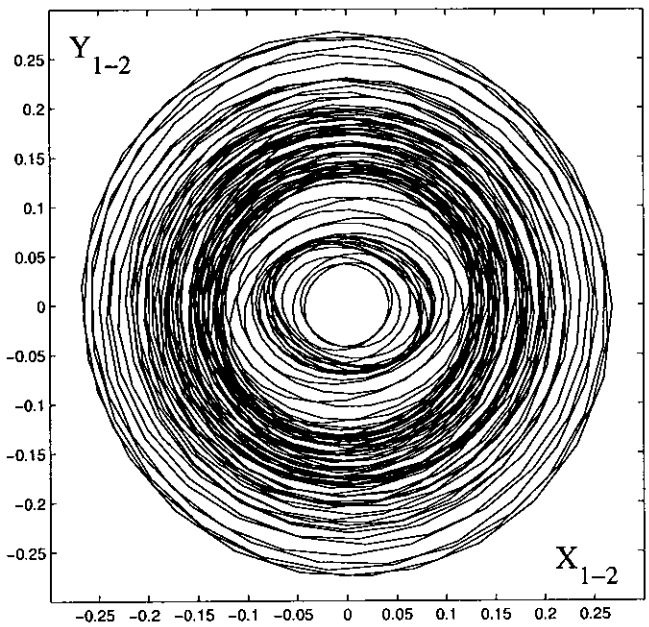

FIG. 7. Trajectory of principal components (1,2) in the complex plane, $Z = X_{1\text{-}2} + iY_{1\text{-}2}$.

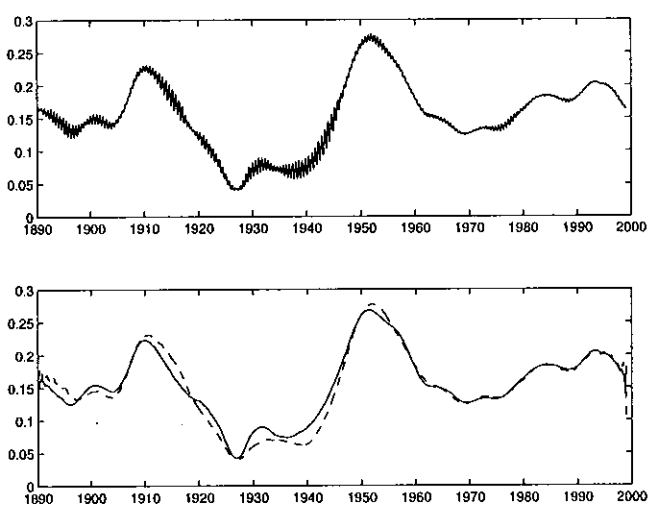

FIG. 8. Top: recomposed time series of $|Z|$. Bottom: Moduli of analytic signals $|X_c|$ (solid line) and $|Y_c|$ (dashes) derived from $X_{1\text{-}2}$ and $Y_{1\text{-}2}$ using the Hilbert transform.

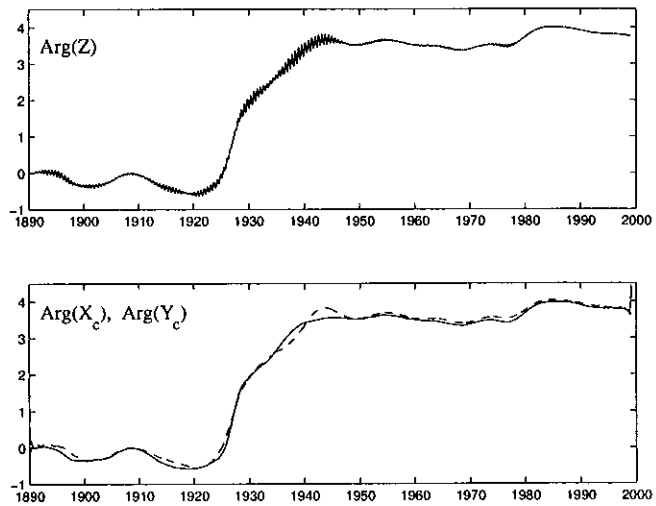

FIG. 9. Top: Argument of $Z = X_{1\text{-}2} + iY_{1\text{-}2}$. Bottom: Arguments of X_c (solid line) and Y_c (dashes). All are corrected from a regular phase-winding corresponding to a period 433 days, which helps one pointing out a phase jump of order π around 1930.

This suggests a phase jump of the order of π in the period [1922, 1942], precisely when the amplitude was small. This feature is also present on the plots, figure 9, of the arguments of the analytical signals X_c and Y_c which are again free of fast oscillation spells affecting Z. The instantaneous rotation rate of the Chandler wobble has been obtained from the time series of $\frac{1}{2}[\arg(X_c) + \arg(Y_c)]$ by differentiation after smoothing it over twenty successive points. Figure 10 displays the corresponding period expressed in days, to be compared with the reference value of 433 days.

5 Length of day (LOD)

The data. The LOD time series is contained in the IERS file C04 [19]. At the time of the study this series started on the 1st of January 1962 and ended on the 4th of July 2000, i.e. 14065 data values. The raw time series is displayed in figure 11 (top panel). The LOD fluctuations contain a quasi-periodic component of astronomic origin due to tide effects that can be computed explicitly by means of a model [20]. The corrected time series is displayed

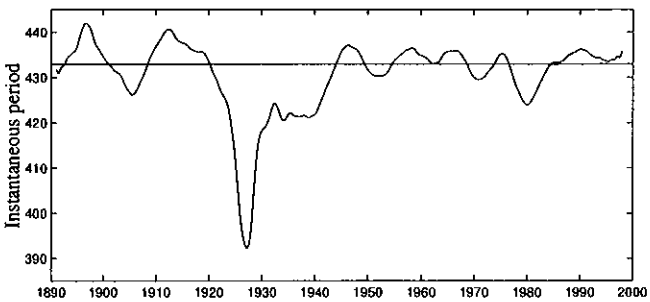

FIG. 10. Instantaneous Chandler period derived from the arguments of the analytic signals $\tilde{X}$ (solid line) and $\tilde{Y}$ (dash-dotted line). The horizontal line corresponds to 433 days.

in figure 11 (middle panel) and the Fourier spectra of the raw and corrected time series displayed in figure 12 show that the tide model is nearly perfect in suppressing the related time dependence. The slow modulation remaining in the corrected time series is eliminated by filtering out its first Fourier coefficients, which yields the series presented in the bottom panel of figure 11 that serves to the subsequent study. It is clearly dominated by a strong seasonal (annual and sub-annual) component already obvious in the Fourier spectra. Here we will rather be interested in the inter-annual variability.

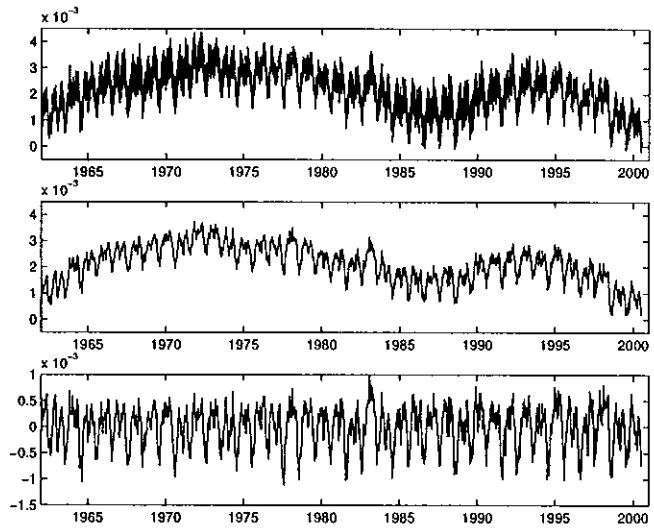

FIG. 11. LOD time series. Top: raw data. Middle: after subtraction of tide effects. Bottom: after filtering of very low frequencies.

The ENSO phenomenon. The principle of angular momentum conservation tells us that the processes immediately susceptible to modify the length of the day originate from the friction of air and water masses in zonal motion on the surface of the solid Earth. These motions take place on variable time scales from few days (meteorology) to several years (climate). In the range of one year or more, the ENSO (acronym of El Niño-Southern Oscillation) phenomenon is one of the most studied. This recurrent major climatic anomaly, developing primarily in the inter-tropical Pacific Ocean, manifests itself as a profound modification of wind regimes and heat exchanges producing an eastward motion of large warm water masses, hence a good candidate to influence LOD variations. Warm (El Niño) and cold (La Niña) episodes alternate with a period varying between 2 and 7 years. Catastrophes at regional

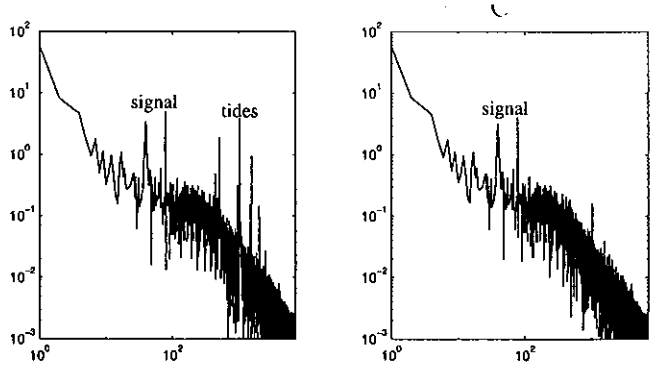

FIG. 12. Fourier spectra of the LOD time series before (left) and after (right) subtraction of tide effects computed according to [20].

and global scales are associated with the most intense El Niño episodes, such as those of 1982–83 or 1997–98 [11].

One of the motivations of V. Fréde's work was the search for a trace of these strong anomalies in the variation of local Lyapunov exponents that measure the predictability of the system [21]. To this 'local' deterministic point of view we shall prefer a more 'global' statistical approach resting on the correlations between the LOD fluctuations and the amplitude of the ENSO cycle. The intensity of this phenomenon is measured by means of several indices that are exploited to predict the short-term risks related to it [22]. Here we have used two indices. The first one is produced by the Japan Meteorological Agency (JMA) as a 5-month sliding average of the see-surface temperature anomaly of that portion of the Pacific Ocean comprised between parallels 4°S and 4°N, and meridians 150°W and 90°W. It is computed from detailed observational data since 1949 but has been estimated from month averages since 1868 [23, a]. The second one, combining several different measurements, is the Multivariate ENSO Index (MEI) produced by K. Wolter at the NOOA Climate Diagnostic Center. It covers the contemporary period since 1950 [23, b].

ENSO–LOD correlation. To fit with the fact that ENSO indices are given as monthly sampled time series we first perform a monthly average of the LOD data. We restrict ourselves to the consideration of the period starting January 1962 and ending November 1999 that corresponds to data available at the beginning of our study, i.e. 455 data pieces.

The seasonal component has been extracted by proceeding to a singular spectrum analysis of a time-delay reconstruction with embedding dimension $d_e = 36$ that corresponds to exactly 3 years of measurements. The spectrum of the covariance matrix is presented in figure 13. It displays two pairs of quasi-degenerated eigen-values that strictly correspond to the expected seasonal contribution to the signal as understood from the aspect of the associated eigen-vectors shown in figure 14 (top). The corresponding recomposed time series is illustrated in figure 15 (top). Next, two pairs of eigen-value

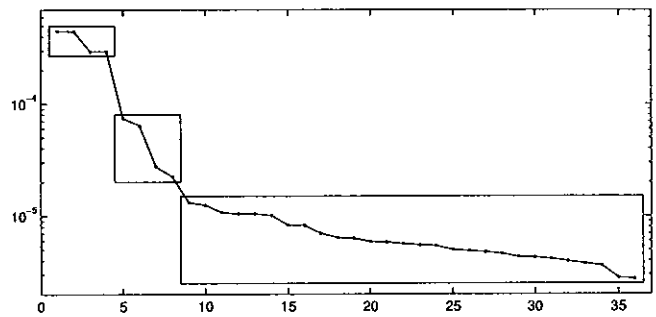

FIG. 13. Spectrum of the covariance matrix of the LOD time series with embedding dimension $d_e = 36$, with indication of the grouping of eigen-values corresponding to the seasonal modulation (1–4), to a non-trivial component (5–8), and to the residue (9–36).

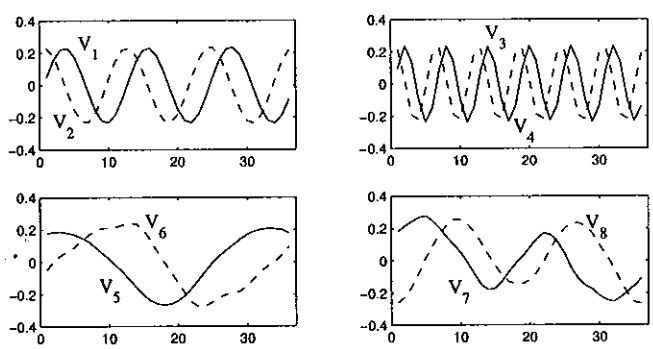

FIG. 14. Eigen-vectors associated with the seasonal variation (eigen-values 1–4) and the nontrivial component (eigen-values 5–8).

appear in the spectrum, slightly detached from a relatively uniform background interpreted as residual 'noise'.

Eigen-vectors associated with eigen-values 5 to 8 are displayed in figure 14 (bottom). The corresponding recomposed time series, hereafter called nontrivial, is shown in the middle panel of figure 15, whereas the remaining signal, recomposed from the eigen-space spanned by vectors 9 to 36, is illustrated in the bottom panel. Fourier analysis of the latter component suggest to consider this as high frequency white noise. [A similar study with embedding dimension twice as large ($d_e = 72$) gives identical results: the seasonal component is still obtained from the four first eigen-values. The same nontrivial component is obtained by recomposition on the

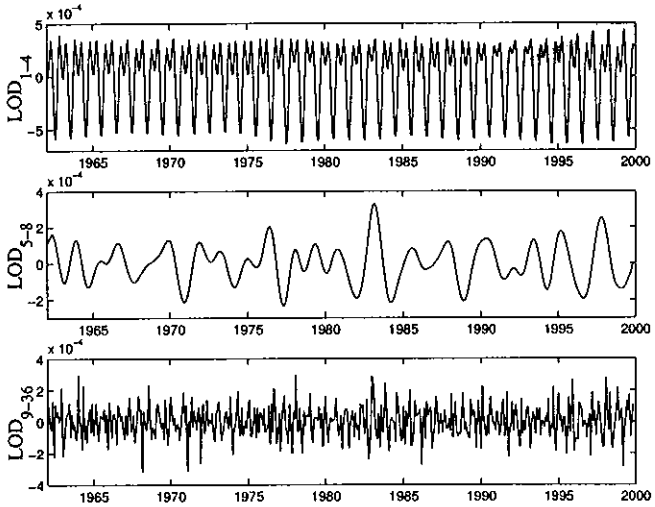

FIG. 15. Reconstructed time series corresponding to the seasonal modulation (principal components 1–4, top), the nontrivial signal (5–8, middle) and the residue (9–36, bottom).

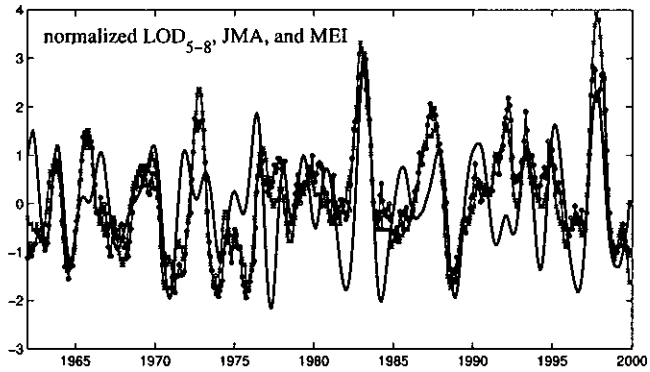

FIG. 16. Correlation between the nontrivial part of the LOD time series extracted by SVD (thick line) and ENSO indices JMA and MEI (thin decorated lines).

space spanned by the six next eigen-vectors (5–10).]

Visual inspection of figure 16 suggests strong correlation between the nontrivial component of the so filtered signal and the ENSO indices JMA and MEI, at least for the the period 1962.5–1971, the most intense El Niño events (1982–83 and 1997–98) and the 1988–89 La Niña event. This can be put on a quantitative footing by computing normalized cross-correlation between them. We obtain 0.511 for the first index and 0.465 for the second (the cross correlation between the two indices is 0.917). These coefficients increase up to 0.531 and 0.495 if the 9 first and last data pieces are dropped, which can be understood as the consequence of spurious end effects in the treatment. The result can even be improved up to 0.543 by a shift of the recomposed time series with respect to the JMA index by one step, the correlation with the MEI remaining constant in the same operation. By contrast the cross-correlation decreases markedly when time series are shifted in one or the other direction by more than one step, which means that the postulated effect is essentially in phase with the suspected cause. In the same way, the correlation decreases as soon as one tries to reconstruct the nontrivial part of the LOD time series by adding the contribution of other principal components or else by removing one of those that have been taken into account in the analysis. So the performed recomposition, using eigen-vectors 5 to 8, achieves some sort of optimum.

6 Discussion

In this work we have analyzed the inter-annual fluctuations of the Earth orientation parameters using techniques derived from the Takens time-delay reconstruction method developed within the framework of the theory of low dimensional dynamical systems. This signal processing exercise explores a range of time scales different from that considered originally by V. Fréde [3] who was rather interested in qualitative aspects of high frequency components of the Chandler wobble and LOD fluctuations and focused primarily on predictability problems *via* the determination of local Lyapunov exponents. We believe that our quantitative results, are at least as convincing as hers, and thus could be of comparable interest to specialists in geodesy or climate dynamics.

In practice, we have been using only the small part of the signal processing techniques based on Takens phase space reconstruction method that makes use of singular value decomposition [6]. Focusing our attention on a specific range of time scales dominated by strong periodicities, we had to worry neither about the optimal sampling time

nor about the most appropriate embedding dimension. These problems become important when dealing with the determination of nonlinear models for prediction purposes, which rather concerns the nonlinear evolution of an autonomous system. By contrast, here the studied signal is essentially the response of a 'simple' mechanical system, a spinning-top, to some 'external' non-stationary forcing. The system is indeed governed by a known set of differential equations equivalent to those for a linear oscillator with (hopefully) known resonance parameters, so that the inversion problem is manageable, which leaves us with the question of identifying the sources of the nontrivial behavior.

In this respect, in addition to a demonstration of feasibility of this kind of approach, we believe that we have obtained some novel and significant information (though we have not scanned the literature sufficiently systematically). In particular, we have explicitly shown that the phase of the Chandler wobble has changed by π around 1930, at a time when the amplitude of the wobble was particularly small. In the same time our approach, especially in figure 10 displaying the instantaneous Earth rotation rate, leads to question the interpretation of its evolution in the relevant frequency range as a linear superposition of several Fourier components. Such an interpretation would be meaningful if these components were to have fixed phase relations that could be freely superposed. On the contrary, here they should have well defined, temporally evolving, phase relations conspiring to build an observed variation which is rather reminiscent of phase defects of driven nonlinear oscillators.

Concerning the LOD data, we have also quantitatively established a strong correlation between its inter-annual variability and the climatic indices measuring the intensity of the ENSO phenomenon. Heuristically, this is satisfactory but the correlation does not explains all the variability. So the question is raised of which phenomena of comparable strength —and possibly of similar origin— could explain the remaining part of the variability. (Another explanation to the lack of full correlation could be that the least-square approximation underlying the SVD step would imply a pinning of the reconstructed time series on its own most intense events and a smooth oscillatory interpolation in-between, so that the discrepancies would rather be an artifact of the method.) Another question to which we have no answer —but it might be obvious to climate specialists— is the reason why, to within not more than one month, the LOD response is strictly in phase with the ENSO triggering, as monitored by the chosen indices and at least for the most intense events (and this, by contrast, cannot be an artifact of the method).

To conclude, our treatment of the data presents itself as a preliminary step before attacking the inverse problem of determining the geophysical contributions to the forcing from the observed time series. The analysis might have its own bias but it suggests that, in the time-scale range considered, the search for a linear superposition of independent processes, implicit in the conventional Fourier-based filtering, is somewhat misleading in view of the evidence of features typical of noisy, low dimensional, dissipative dynamical systems. The outlines of an interesting program for future work are therefore drawn but, unfortunately, this program lies somewhat beyond our field of competence and will thus be left to specialists.

Enlightening discussions with Valrie Fréde and the participation of Peggy Cenac to early developments of this work are deeply acknowledged.

References

[1] H.D.I. Abarbanel. *Analysis of Observed Chaotic Data.* (Springer-Verlag, Heidelberg, 1996).

[2] H. Kantz, Th. Schreiber. *Nonlinear Time Series Analysis.* (Cambridge Nonlinear Science Series 7, Cambridge, 1997).

[3] V. Frède. Apport de l'analyse non linéaire l'étude géophysique de la rotation de la terre. (PhD Thesis, Observatoire de Paris, 1999); V. Frède, P. Mazzega. Detectability of deterministic non-linear processes in Earth rotation time-series —I. Embeddings, II. Dynamics. Geophys. J. Int. **137**, 551–564 & 565–579 (1999); V. Frède, P. Mazzega. A preliminary nonlinear analysis of the Earth's Chandler wobble.

Discrete Chaotic Dynamics in Nature and Society. **4** (1999).

[4] International Earth Rotation Service (IERS), Observatoire de Paris, 61, avenue de l'Observatoire, F-75014 Paris, France, `http://hpiers.obspm.fr`

[5] F. Takens. Detecting strange attractors in turbulence. Lect. Notes Math. **898**, 366–381 (1981). see also: N.H. Packard *et al.* Geometry from a time series. Phys. Rev. Lett. **45**, 712–716 (1980).

[6] D.S. Broomhead, G.P. King. Extracting qualitative dynamics from experimental data. Physica D. **20**, 217–236 (1986).

[7] R. Vautard, M. Ghil. Singular spectrum analysis in nonlinear dynamics, with applications to paleoclimatic time series. Physica D. **35**, 395–424 (1989); R. Vautard, P. Yiou, M. Ghil. Singular spectrum analysis: a toolkit for short, noisy chaotic signals. Physica D. **58**, 95–126 (1992).

[8] see, e.g. F.D. Stacey, *Physics of the Earth.* (Wiley, New York, 1969). Chapter 2.

[9] Conference *Polar motion: Historical and Scientific problems*, IAU Colloquium 178, Cagliari, 27–30 September 1999; `http://maia.usno.navy.mil/iauc19/ abstracts/ program.html`

[10] R.S. Gross. The excitation of the Chandler wobble. Geophys. Res. Lett. **27**, 2329–2332 (2000).

[11] For an introduction see: J.P. Peixoto, A.H. Oort. *The physics of climate.* (American Institute of Physics, NY, 1992). Pp. 415 and following. A more detailed description of the phenomenology can be found in the first chapters of: S.G. Philander. *El Niño, La Niña, and the Southern Oscillation.* International Geophysics Series. **46** (Academic Press, San Diego, 1990).

[12] T. Sauer, J.A. Yorke, M. Casdagli. Embedology. J. Stat. Phys. **65**, 579–616 (1991).

[13] A.M. Fraser, H.L. Swinney. Independent coordinates for strange attractors from mutual information. Phys. Rev. A. **33**, 1134–1140 (1986).

[14] M.B. Kennel, R. Brown, H.D.I. Abarbanel. Determining embedding dimension for phase-space reconstruction using a geometrical construction. Phys. Rev. A. **45**, 3403–3411 (1992) (and references quoted).

[15] see e.g. A. Papoulis. *Signal analysis.* (McGraw-Hill, New York, 1977). Chapter 7.

[16] in directory `http://hpiers.obspm.fr/ iers/ eop/ opc01/`.

[17] The value of the fitting coefficients have no interest in themselves but can be communicated upon request. We used polynomials of degree 6 to remove the trend (MatLab functions `polyfit.m` and `polyval.m`) and Fourier harmonics up to the 4th for the annual and subannual oscillations (routine `lfit` from *Numerical Recipes in Fortran* by Press *et al.*, Cambridge University Press, 1992).

[18] Spurious oscillations, hardly visible in the figure, appear at the very beginning and the very end of the times series of the moduli and arguments of X_c and Y_c, due to end effects when taking the Fourier transforms to obtain these quantities.

[19] in directory `http://hpiers.obspm.fr/ iers/ eop/ opc04/`.

[20] implemented as the IERS FORTRAN routine `cmarot.f`, see `http://hpiers.obspm.fr/ webiers/ general/ communic/ mod/ CMAROT_T.html`

[21] B. Eckhardt, D. Yao. Local Lyapunov exponents in chaotic systems. Physica D. **65**, 100–108 (1993).

[22] M. Ghil, M. Kimoto, J.D. Neelin. Nonlinear dynamics and predictability in the atmospheric sciences. Review of Geophysics Supplement. 46–55 (1991).

[23] (a) Japan Meteorological Agency, index `jmasst1868-today.filter-5` in directory `ftp://www.coaps.fsu.edu/ pub/ JMS_SST_Index/`; (b) NOOA Climate Diagnostics Center, multivariate ENSO index (MEI data: courtesy K. Wolter), `http://www.cdc.noaa.gov/~kew/MEI/`